Computers and Geotechnics. Submitted January 2017; Published January 2018.
http://dx.doi.org/10.1016/j.compgeo.2017.05.013

Numerical analysis of Ballina test embankment on a soft structured clay foundation

Mohammad Rezania [*,1], Hung Nguyen [†], Hossein Zanganeh [†], Mahdi Taiebat [§]

[*] School of Engineering
The University of Warwick
Coventry, CV4 7AL, UK
E-mail: m.rezania@warwick.ac.uk

[†] Department of Civil Engineering
The University of Nottingham
Nottingham, NG7 2RD, UK
E-mail: hung.nguyen@nottingham.ac.uk
E-mail: hossein.zanganeh@nottingham.ac.uk

[§] Department of Civil Engineering
The University of British Columbia
Vancouver BC V6T 1Z4, Canada
Email: mtaiebat@civil.ubc.ca

Abstract: This paper focuses on numerical modeling of the responses of Ballina test embankment by an improved EVP-SANICLAY constitutive model with a novel rotational hardening (RH) law. The modified RH law guarantees the uniqueness of the critical state line, prevents excessive rotation of yield surface and is particularly simple that makes it very useful for practical applications. To consider strain-rate dependency of the soil behavior, Perzyna's overstress theory is employed. Using the newly released data at Ballina test embankment site, the values of model parameters and state variables are calibrated and evaluated for Class C predictions, and their differences with the previously determined parameter values for Class A predictions are highlighted and discussed. The elasto-viscoplastic anisotropic constitutive model is implemented in PLAXIS software to carry out the simulations of the case study

[1] Corresponding author. Tel.: +44 24 765 22339.

Computers and Geotechnics. Submitted January 2017; Published January 2018.
http://dx.doi.org/10.1016/j.compgeo.2017.05.013

embankment. The numerical modeling results, in terms of time-dependent variations of deformations and pore water pressures, both during and after the embankment construction, are compared with the physical measurements at the test site. The results of Class C analyses show that the model is capable of capturing the temporal changes in surface settlement and lateral deformations with good accuracy, with the latter being particularly challenging when modeling the behavior of soft clays. Simulation of pore water pressure variations however proved more difficult. To highlight the advantages of the proposed EVP-SANICLAY model, the simulations are also compared with those using the classical Mohr-Coulomb and modified Cam-clay models, and the results are presented and discussed in detail.

Keywords: Viscoplasticity; Ballina embankment; Clay anisotropy; Vertical drains.

1. INTRODUCTION

Despite significant developments in the past few decades, modeling, design and construction on soft soils are still challenging for geotechnical engineers, since their response is governed by a series of fundamental features that are not always included in conventional constitutive models. Any realistic constitutive model development for soft soil behavior should account for their inherent features such as anisotropy, destructuration (degradation of the inter-particle bonds), and time-dependency. Soil anisotropy can be modeled by development of elastoplastic constitutive models involving an inclined yield surface that is either fixed (e.g., [1]), or can change its inclination by adopting a rotational hardening (RH) law in order to simulate the development or erasure of anisotropy during plastic straining (e.g., [2, 3]). Dafalias and Manzari[4] proposed what they called SANICLAY model, altering the original RH law introduced by Dafalias in [2] and adopting a nonassociated flow rule. A destructuration theory was later applied to the SANI-CLAY model to account for both isotropic and frictional

destructuration processes [5]. Capabilities of the SANICLAY model and its variants have been illustrated in successful simulation of drained and undrained responses of normally consolidated and overconsolidated sensitive clays [6,7] and applications in boundary value problems [8,9].

Time-dependency is another typical feature of soft clays behavior which has widely been experimentally observed [10-12] and is usually considered a function of soil viscosity. Time-dependency can result in particular effects such as creep, stress relaxation, and strain-rate dependency of the soil response. For experimental investigation of time-dependency creep tests, stress relaxation tests, or constant rate of strain (CRS) tests can be used [13]. For common practical problems, such as embankments on soft soils, a sustainable design solution can only be achieved if time-dependent behavior of soil is taken into consideration. To do so, different frameworks can be applied [14], among which the overstress theory of Perzyna [15] is a common framework often used in geomechanics owing to its relative simplicity. Recently, Rezania et al. [16] developed a new Elasto-ViscoPlastic SANICLAY (EVP-SANICLAY) model in which they considered the rotational hardening and destructuration features of SANICLAY model for simulation of anisotropy and sensitivity, respectively, and also employed Perzyna's overstress theory to account for soil viscosity effects. The EVP-SANICLAY model is therefore the new member of the SANICLAY family of models.

In this paper, the RH law in the newly developed EVP-SANICLAY model has been further simplified, and the modified model has been examined in predicting the responses of Ballina test embankment. The layout of the paper is as follows. First, the modified EVP-SANICLAY model and its new RH law are described in Section2.In Section3, the parameters of the model are evaluated and calibrated. Then, in Section4, the numerical modeling of the Ballina test embankment and its predicted responses are presented and analyzed.

Computers and Geotechnics. Submitted January 2017; Published January 2018.
http://dx.doi.org/10.1016/j.compgeo.2017.05.013

2. EVP-SANICLAY MODEL

The incremental viscoplastic strains $\Delta\boldsymbol{\varepsilon}^{vp}$ in the EVP-SANICLAY [16] model can be calculated as:

$$\Delta\boldsymbol{\varepsilon}^{vp} = \dot{\boldsymbol{\varepsilon}}^{vp}.\Delta t = \mu\langle \Phi(F)\rangle \frac{\partial g}{\partial \boldsymbol{\sigma}}.\Delta t \tag{1}$$

where $\dot{\boldsymbol{\varepsilon}}^{vp}$ is the viscoplastic strain rate tensor (the overdot denotes the time derivative). μ is referred to as the fluidity parameter; $\langle\ \rangle$ are McCauley brackets which imply that only positive values are taken into consideration and negative values are taken as zero; g is the viscoplastic potential function, represented by the dynamic loading surface (DLS) as explained in the following. $\Phi(F)$ is the overstress function representing the difference between the DLS and the current static yield surface (SYS). Figure 1(a) shows the schematic SYS of the SANICLAY model in the general stress space. For the scaling function an exponential form proposed by [17] can be adopted

$$\Phi(F) = \exp(F) - 1 = \exp\left[N\left(\frac{p_0^d}{p_0^s} - 1\right)\right] - 1 \tag{2}$$

where p_0^s and p_0^d are representing the sizes of the SYS and the DLS, respectively; N is the strain-rate coefficient that together with μ are the two viscous parameters of this model.

Knowing the incremental viscoplastic strains, using Perzyna's overstress theory [15], the total strain increment can be defined as the summation of the elastic strain increment $\Delta\boldsymbol{\varepsilon}^{e}$ and the viscoplastic strain increment

$$\Delta\boldsymbol{\varepsilon} = \Delta\boldsymbol{\varepsilon}^{e} + \Delta\boldsymbol{\varepsilon}^{vp} \tag{3}$$

The elastic strain increment is time-independent; whereas, the viscoplastic strain increment, $\Delta\boldsymbol{\varepsilon}^{vp}$, is irreversible and time-dependent. The elastic part of the total strain, using isotropic hypoelastic relations, can be shown as

Computers and Geotechnics. Submitted January 2017; Published January 2018.
http://dx.doi.org/10.1016/j.compgeo.2017.05.013

$$\Delta\boldsymbol{\varepsilon}^e = \boldsymbol{D}^{-1}{:}\,\Delta\boldsymbol{\sigma} \tag{4}$$

where $\boldsymbol{D}$ is the elastic stiffness matrix and symbol : implies the trace of the product of two tensors. The hypoelastic formulation, constitutes of a shear modulus G, for calculating increments of elastic deviatoric strains, and a bulk modulus K, for calculating increments of elastic volumetric strains

$$G = \frac{3K(1-2\nu)}{2(1+\nu)}; \quad K = \frac{p(1+e)}{\kappa} \tag{5}$$

where ν is the Poisson's ratio; e is the void ratio; $p = (\mathrm{tr}\boldsymbol{\sigma})/3$ is the mean effective stress (where tr stands for the trace), and κ is the slope of elastic swelling lines in the e-ln$p$ space.

In the general stress space, the SYS function can be expressed as

$$f^s = \frac{3}{2}(\boldsymbol{s}-p\boldsymbol{\alpha}){:}\,(\boldsymbol{s}-p\boldsymbol{\alpha}) - \left(M^2 - \frac{3}{2}\boldsymbol{\alpha}{:}\,\boldsymbol{\alpha}\right)(p_0^{*s}-p)p = 0 \tag{6}$$

In the above expression, $\boldsymbol{s} = \boldsymbol{\sigma} - p\boldsymbol{I}$ is the deviatoric component of stress tensor $\boldsymbol{\sigma}$ ($\boldsymbol{I}$ being the second-order identity tensor). $\boldsymbol{\alpha}$ is the deviatoric fabric tensor that accounts for anisotropy by coupling the deviatoric and volumetric plastic strain rates. $p_0^{*s} = S_i P_0^s$ defines the size of the structured SYS where $S_i > 1$ is an isotropic destructuration factor and P_0^s is the size of the intrinsic SYS, and M is the critical stress ratio. As shown in Figure 1(b), the DLS has the same shape and orientation as the smaller SYS, and following the adoption of associated flow rule it coincides the viscoplastic potential surface too.

The isotropic hardening law of the model describing the evolution of the size of structured SYS, i.e. p_0^{*s}, is defined as

$$p_0^{*s} = \dot{S}_i p_0^s + S_i \dot{p}_0^s = 0 \tag{7}$$

Computers and Geotechnics. Submitted January 2017; Published January 2018.
http://dx.doi.org/10.1016/j.compgeo.2017.05.013

where $\dot{S}_i$ is the evolution rate of the isotropic destructuration factor, and $\dot{p}_0^s = [(1+e)/(\lambda-\kappa)]p_0\dot{\varepsilon}_v^{vp}$ is the evolution of the size of SYS, that is proportional to viscoplastic volumetric strain rate, with λ indicating the slope of normal compression line.

To describe the evolution of fabric anisotropy with viscoplastic straining, a new rotational hardening law proposed by Dafalias and Taiebat [18] is employed which is expressed as

$$\dot{\boldsymbol{\alpha}} = \langle L \rangle c p_{at} \frac{p}{p_0}(\boldsymbol{\alpha}_b - \boldsymbol{\alpha}) + \dot{\boldsymbol{\alpha}}_f; \quad \boldsymbol{\alpha}_b = \pm\frac{M}{z}\left[1 - \exp\left(s\frac{|\boldsymbol{\eta}|}{M}\right)\right] \tag{8}$$

where L is the plastic multiplier, c is a model parameter controlling the pace of evolution of $\boldsymbol{\alpha}$ to its bounding value $\boldsymbol{\alpha}_b$, and z and s are the model constants controlling the equilibrium values of $\boldsymbol{\alpha}$ under constant-stress-ratio $\boldsymbol{\eta}$ loadings.

The $\dot{\boldsymbol{\alpha}}_f = (\dot{S}_f/S_f)\boldsymbol{\alpha}$ controls the contribution of destructuration over the change of orientation of the yield surface. In order to express the isotropic and frictional destructurations, an axillary internal variable called the destructuration viscoplastic strain rate, $\dot{\varepsilon}_d^{vp}$ is defined by

$$\dot{\varepsilon}_d^{vp} = \sqrt{(1-A)\dot{\varepsilon}_v^{vp\,2} + A\dot{\boldsymbol{\varepsilon}}_q^{vp\,2}} \tag{9}$$

where $\dot{\varepsilon}_v^{vp}$ and $\dot{\boldsymbol{\varepsilon}}_q^{vp}$ are the volumetric and deviatoric viscoplastic strain rates, respectively, and A is a model parameter which could be set to 0.5 as a default value [5]. The evolution equations for the S_i and S_f read

$$\dot{S}_i = -k_i\left(\frac{1+e}{\lambda-\kappa}\right)(S_i - 1)\dot{\varepsilon}_d^{vp} \tag{10}$$

$$\dot{S}_f = -k_f\left(\frac{1+e}{\lambda-\kappa}\right)(S_f - 1)\dot{\varepsilon}_d^{vp} \tag{11}$$

where k_i and k_f are additional model parameters.

Computers and Geotechnics. Submitted January 2017; Published January 2018.
http://dx.doi.org/10.1016/j.compgeo.2017.05.013

The numerical solution algorithm for the elasto-viscoplastic model can be developed by using a step-by-step time integration scheme with a Newton-Raphson iteration procedure, as described in [16].

3. EVALUATION OF MODEL PARAMETERS AND MODEL CALIBRATION

The model constants of EVP-SANICLAY can be divided into 5 categories: 1) the elasticity constants κ and ν; 2) the critical state constants λ and M (slope of critical state line) (CSL), which are the same as those in the MCC model; 3) the RH constants c and s, which are specific to the SANICLAY model; 4) the destructuration constants k_i and k_f which are also specific to the SANICLAY model; 5) the viscosity parameters N and μ, which constitute the two time-effect parameters of the EVP-SANICLAY and they can be determined as discussed in [16]. Some of the model parameters, such as κ, M and λ_i (the intrinsic value of λ), can be directly evaluated through the results of element level tests while some others, such as c and k_i can be evaluated through calibration using element level test data. In this section the procedures undertaken to evaluate the model parameters for Ballina clay at three different depths of the soft soil deposit (1.5-4.8, 4.8-8.7, and 8.7-10.7m) [19] are explained. It should be mentioned that in [20] the model parameter values were evaluated based on limited number of CRS and triaxial test results which were provided for each soil layer. In the present work, the supplementary experimental data, which were provided after the *Embankment Prediction Symposium* (EPS) *2016* [21], are also used for an improved determination of the parameters.

3.1 Determination of soil parameters

The parameters κ and λ_i can be obtained from the results of isotropic or one-dimensional compression tests presented in e–log p space. Here, the experimental data of CRS tests provided for and after EPS [21] are used to obtain the elasticity parameter κ, and the critical

state constant λ_i. Figures 2 (a) and (b) show the experimental results and the lines fitted to the data for clay samples taken from the depth of 6.63m. As it can be seen in Figure 2(a), three swelling lines result in three different values of κ, hence an average value is selected for the simulation of the test embankment. The slope of the fitted line to the latter part of the compression curve plots is taken as λ_i [5], (see Figure 2(b)). The experimental results of the CRS tests are also used for the evaluation of the initial isotropic structuration factor S_{io}. As it is explained in [18] and is illustrated in Figure 2(c), S_{io} is equal to the difference between effective vertical stress of the remoulded clay and that of the structured clay corresponding to the void ratio of the yield point in the CRS test. Using the new data, the value of S_{io} at the depth of 6.63m shows 5% change compared to its previous value used in [20].

The slope of CSL is obtained through triaxial tests. Figure 3 illustrates how the results of undrained shearing of triaxial samples are used for the evaluation of M. As it is seen in this figure, a first order polynomial with zero y-intercept is fitted to the portion of the test in which shearing occurs and the slope of that line is reported as M. The initial size and inclination of SYS depend on the stress-strain history of the soil deposit. For Class A predictions in [20] α_0 was calibrated by passing it through the initial stress point of the triaxial test. In the present work, α_0 is directly evaluated using the formula suggested by [22]

$$\alpha_0 = \frac{\eta_{K0}^2 + 3\eta_{K0} + M^2}{3} \tag{12}$$

where η_{K0} is the stress ratio corresponding to K_0. When the initial value of α is chosen, the other RH parameters $z = s$ can be calculated by Eq. (11) of [18]. The remaining anisotropy, destructuration and viscosity parameters are calibrated against experimental results, as explained in the sequel.

Computers and Geotechnics. Submitted January 2017; Published January 2018.
http://dx.doi.org/10.1016/j.compgeo.2017.05.013

3.2 Calibration of additional model parameters

To calibrate the initial rate of the isotropic destructuration k_i and viscosity parameters N and μ the CRS element test results are used. To perform these calibrations, the model has been implemented into PLAXIS AE software, through its user-defined soil model facility [23], and used for element level tests simulations. In Figure 4(a), the numerical results are compared with the experimental oedometric data of the soil samples taken from depth of 6.63m of Ballina deposit. This figure illustrates that the choice of the initial value of k_i does not drastically affect the results. Similarly, the calibration procedure for viscosity parameters N and μ is illustrated in Figure 4(b). It should be pointed out that the Perzyna-type viscosity parameters for a particular clay are not necessarily a unique set [16]. As it was indicated in [20] more experimental results will lead to a better calibration of these parameters. Hence, with the new results provided for the Ballina clay deposit, new values are suggested for these parameters.

Using the triaxial test results, the remaining parameters of c, k_f and S_{f0} are also calibrated. For Class A predictions, these calibrations were done by simulating stress path tests and comparing the numerical results with experimental data. In the present work, the calibrations have been done by comparing model predictions with experimental results of deviatoric stresses versus axial strains. The trial simulations to calibrate these parameters, together with the corresponding experimental data, are shown in Figure 5. Based on the authors' experience from extensive element level simulations, the effect of RH constant c on the numerical predictions is minimal, k_f variations only affect the numerical predictions when the sample state is on the CSL and almost the entire stress path is affected by S_{f0} variations.

3.3 Discussion on the model parameters and constants

For EVP-SANICLAY model, the values of 10 model parameters and the initial values of 5 state variables should be determined. These constants can be categorized into four different

groups of:

- Model constants $M, \lambda, \kappa, \nu, e_0$ and OCR/POP which are similar to the MCC model parameters and are widely used in critical sate based constitutive models. The values of these parameters can be directly obtained from standard laboratory tests. While OCR and POP may not be considered as standard MCC parameters; however, as it will be discussed in the sequel the initial size of the yield surface, which is one of the main state variables of MCC model, is often calculated based on OCR or POP values.
- Initial anisotropy and RH constants which simulate the evolution of soil anisotropy. The initial orientation of soil fabric can be described through a fabric tensor. For practical purposes, in modelling the initial orientation of soil's fabric is often considered to be of cross-anisotropic nature which is a realistic assumption as natural soils have been generally deposited only one dimensionally in a vertical direction [24]. This assumption simplifies the initial calculation of fabric tensor components, which can therefore be determined using a scalar value α_0 that represents the initial orientation of the yield surface.
- Destructuration parameters which can be calibrated using K_0, or isotropic consolidation tests results (for k_i and S_{i0}) and undrained triaxial tests (for k_f and S_{f0}).
- Viscosity parameters N and μ which can be determined using long-term oedometer test results, and/or CRS test data.

Most of these parameters represent actual physical properties of the soil. Hence, evaluation and calibration of these parameters can be done through a straightforward procedure. Following the parameter calibration procedure discussed in the previous section, the values of the model parameters for the soil samples taken at two other depths of 1.5-4.8m, and 8.7-10.7m and a sandy-clayey silt layer, have also been obtained. In this work, the parameter values are assumed to be constant in depth. Hence, the evaluated model parameters for three different depths are

Computers and Geotechnics. Submitted January 2017; Published January 2018.
http://dx.doi.org/10.1016/j.compgeo.2017.05.013

averaged and a single value for each parameter is reported in Table 1. In the following section, these parameters are applied for the numerical simulation of the embankment.

For a better illustration of the changes made to parameter values for Class C predictions, compared to the values used for Class A predictions, for each parameter and state variable both values are reported in Table 1. As values in the table indicate, most of the parameters show only a minimal alteration of less than 10%, for the viscosity parameter N which shows a more distinctive change, the values are still of the same order. Overall, these changes are the outcome of (i) new evaluation procedures, as it is the case for α_0, and (ii) availability of the complimentary experimental results provided after the EPS [21], as it is the case for the parameters such as N and M. In addition to these changes, the procedure through which the model uses the preconsolidation pressure for boundary value simulation has been changed. For Class A predictions, the preconsolidation pressure was directly fed into the model; hence the initial state of each soil layer was represented with a single preconsolidation pressure. Based on the authors' experience [16], while using p_0^{*s}, as one of the model input parameters, improves the performance of the model in element level simulations, for the boundary value problems, such as embankment simulations, p_0^{*s} is better to be evaluated indirectly through overconsolidation ratio (OCR) or pre-overburden pressure (POP) values. This is mainly due to the fact that the value of p_0^{*s} depends on the previous stress-strain states of the soil which varies with the variation of the soil depth. Using OCR or POP lets one to account for this variation while direct application of p_0^{*s} overlooks its variations. In the present work, POP is used for this purpose.

Computers and Geotechnics. Submitted January 2017; Published January 2018.
http://dx.doi.org/10.1016/j.compgeo.2017.05.013

4. EMBANKMENT MODELING

In the following, the modified EVP-SANICLAY constitutive model is used to predict the performance of the case study embankment built on the soft Ballina clay deposit and the results are explained in detail.

4.1 Model description

Ballina test embankment is constructed in Ballina, NSW, Australia, it is 3m high and 80m long with a side slope of 1:2.5. The width of the embankment at the top is 16m. The embankment material is high plasticity clay derived from basalt cuttings. It is constructed on 9.2m deep layer of Ballina clay, underlain by clayey sand to medium sand layers down to a depth of 19.3m. The soft deposit is overlain by approximately 1.5m alluvial clayey silt. To study the performance of new Jute prefabricated vertical drains (PVD), half of the test embankment was constructed on the ground improved by Jute PVDs and the other half was constructed on the ground improved by conventional PVDs. The latter is the focus of this paper. The instrumentation of Ballina test embankment included several settlement plates, inclinometers, magnetic extensometers, total and push in pressure cells, hydrostatic profile gauges and numerous pore pressure probes [21].

For the numerical analysis, the embankment itself is modeled with the simple linear elastic-perfectly plastic Mohr-Coulomb (MC) model using the following values for the embankment material: Young's modulus E = 25,000 kPa, Poisson's ratio ν = 0.25, friction angle ϕ = 38°, and cohesion c = 1 kPa. The sandy-clayey silt layer above, and the sensitive Ballina clay deposit below the water table are modeled in PLAXIS using the EVP-SANICLAY model implemented as a user-defined model. The clayey sand layer below the Ballina clay deposit is also modeled with the MC model using Young's modulus E = 10,000 kPa, Poisson's ratio ν = 0.25, friction angle ϕ = 30°, and cohesion c = 2 kPa. Similarly, the underlying medium sand layer is also

Computers and Geotechnics. Submitted January 2017; Published January 2018.
http://dx.doi.org/10.1016/j.compgeo.2017.05.013

simulated with the MC model using Young's modulus E = 40,000 kPa, Poisson's ratio ν = 0.25, friction angle ϕ = 35°, and cohesion c = 1 kPa. These parameters are also summarized in Table 2.

In this work, a two-dimensional (2D) plane strain finite element model of the embankment is created using PLAXIS, and taking advantage of the symmetry, only half of the embankment is modeled. The six-noded triangular elements are employed (see Figure 6) and large strain analysis has been carried out for all simulations to take into account the buoyancy of the fill material as they become submerged during consolidation. Each element has pore water pressure (PWP) degrees of freedom at corner nodes. The effect of PVDs in the numerical model is taken into consideration. It should be mentioned that, to consider the effects of vertical drains, often the permeability of an entire soil layer in which PVDs are installed in only a part of it, is modified for plane strain simulations (e.g., [25]). However, based on the authors' experience and extensive numerical simulations carried out, in the opinion of the authors it is only the permeability of the soil in the vicinity of the PVDs that should be modified.

For the Class A simulations, while the subsoil deposit underneath the embankment was modified by adding vertical drains in the PLAXIS model, an equivalent horizontal permeability k_{he} for the surrounding soil was calculated using the equation proposed by [26]:

$$\frac{k_{he}}{k_h} = \frac{{D_e}^2}{6R^2\left[\ln\frac{D_e}{D_s} + \frac{k_h}{k_s}\ln\frac{D_s}{D_w} - \frac{3}{4}\right]} \tag{13}$$

where D_e is the diameter of unit cell as D_e=1.13S = 1.13 × 1.2 = 1.36m in which S is the space between the drains [27]. D_w and D_s are the equivalent diameters of the drain and the smear zone, respectively. Following the suggestion by [28], the equivalent diameter of the drain can be estimated as 0.454w in which w is the width of the drain, hence D_w = 0.454m. $k_h$and k_s are the horizontal hydraulic conductivity of the undisturbed and smeared soil, respectively. Eq. (13) shows that to calculate the equivalent horizontal permeability for the PVD-improved

subsoil, the two key parameters of the smear zone (D_s/D_w and k_h/k_s) shall be evaluated. However, no data had been provided to fulfil this requirement. Though the extent of these parameters can be found through similar studies in the literature. For instance, [29] and [30] proposed that D_s can be 5-8 times of the equivalent diameter of the drain. Madhav et al. [31] conducted different tests on the soil specimens collected from the field at different distances from the drains and concluded that the hydraulic conductivity of the soil surrounding the drain is reduced by 5 times compared to that of the undisturbed soil. Also, [32] recommended k_h/k_s to be between 5 and 20 for Bangkok clay. Hence, for the Class A simulations, D_s/D_w was assumed to be equal to 8 and a value of 20 was used for k_h/k_s.

The procedure used for the Class A predictions, as it is explained by [33] increases the numerical cost of the analysis and is time-consuming. Hence, for the Class C predictions, rather than adding vertical drains in the PLAXIS model, an equivalent vertical permeability k_{ve} is used for the PVD-improved subsoil using the simple formula proposed by [34]. This method considerably reduces the simulation time (more than five times faster) as the subsoil deposit underneath the embankment is modeled as a normal soil with a modified permeability. The equivalent vertical permeability is calculated as follows:

$$k_{ve} = \left(1 + \frac{1.5l^2}{\mu D_e^2}\frac{k_h}{k_v}\right)k_v \tag{14}$$

where l is the drainage length, k_v is the vertical hydraulic conductivity of the natural soil and μ is determined by the following equation:

$$\mu = \ln\frac{n}{s} + \frac{k_h}{k_s}\ln s - \frac{3}{4} + \pi\frac{2l^2k_h}{3q_w} \tag{15}$$

where $n = D_e/D_w$, $s = D_s/D_w$ and $q_w = 2522.8\ \mathrm{m}^3/\mathrm{year}$ is the discharge capacity of PVD [21]. For the Class C predictions that the field measurements of the embankment responses are available, the D_s/D_w and k_h/k_s are determined via back calculations, and the respective values of 7.5 and 18 are found suitable for them for the numerical analyses of the next section. It is

worth mentioning that the equivalent horizontal permeability is still obtained using the formula suggested by [26].

As stated above, for the boundary value simulations the PLAXIS calculation mode for large strain analyses with updated pore pressures was selected in which the soil permeability changes during consolidation analysis as the permeability of soil layers varies with the variation of void ratio. The variation of permeability with void ratio is modeled with the simple so-called Taylor's equation [35],

$$\log\frac{k}{k_0} = \frac{\Delta e}{c_k} \tag{16}$$

where k_0 is the initial permeability of the soil, k is the permeability of the soil in the calculation step, Δe is the void ratio variation and c_k is the permeability change index. The permeability parameters used for each soil layer in Class A and Class C simulations are summarized in Table 3. It should be noted that in this study, for all numerical simulations (i.e. using MC, MCC and EVP-SANICLAY models) the same permeability values have been used.

The far-right boundary of the model is assumed at a distance of 50m from the embankment centreline. The bottom boundary of the soil strata is assumed to be completely fixed in both horizontal and vertical directions, whereas, the left and right vertical boundaries are only restrained horizontally. Drainage is allowed at the ground level. Impermeable drainage boundaries are assigned to the lateral and bottom boundaries. Based on ground data, water table is assumed at the depth of 1.2m. Mesh sensitivity studies have been carried out to ensure that the mesh intensity will not affect the accuracy of the results. The numerical predictions of the embankment behavior are presented and discussed in the following section.

4.2 Numerical predictions

The Class C numerical analyses performed with modified EVP-SANICLAY are presented in this section. The results are accompanied with their corresponding Class A predictions. The

differences between these two classes of predictions are mainly due to the fact that, in the present work with the disclosure of actual field measurements, the model parameters are updated (using also the new supplementary experimental results data); furthermore, in the new implementation of the constitutive model the variation of preconsolidation pressure with depth is accounted for, and also the equivalent permeability of the PVD improved soil is evaluated with a new approach. For comparison and better highlighting the capabilities of EVP-SANICLAY model, the test embankment has also been analyzed with commonly used MC and MCC models. The parameter values used for MC and MCC simulations are summarized in Tables 2 and 4, respectively. As it was mentioned earlier, similar sets of permeability values (Table 3) have been used for all three different models studied in this work. Therefore, the differences in the results cannot be associated with different permeability values.

Figures 7(a and b), (c and d) and (e and f) show the Class A and Class C settlement predictions versus time during embankment construction, field observation period, and after a long period of time, respectively. The settlement is measured at a node at the bottom of the embankment (point A in Figure 6) which corresponds to the location of SP2 settlement plate of the instrumentation setup. Along with the numerical results of EVP-SANICLAY model, the results of MC and MCC models are also shown. Figures 7(a) and (b) illustrate that the short-term predictions of all three models (within 10 days of embankment construction) are qualitatively comparable. Quantitatively, for the Class C simulations, EVP-SANICLAY settlement predictions are larger than those from the MC model, but similar to MCC predictions. Within this timeframe all three models overestimate the settlement of the embankment. In the following construction phases and within the first 40 days, similar trends can be observed. However, as time passes and effects of soil characteristics such as anisotropy, sensitivity and time-dependency on the embankment response become more pronounced, notable differences emerge in the numerical results. For instance, the settlement doubles within

the next 5 days by increasing from 0.05m to 0.12m from day 40 to day 45, respectively. This increase results in a better match between the experimental data and the corresponding numerical predictions of the EVP-SANICLAY and MCC models.

The comparison of the results shown in Figures 7(c) and (d) shows that the new set of model parameters used for Class C predictions have increased the magnitude of settlement predicted by all three models. However, while the MC and MCC models clearly fail to predict the settlement of the embankment within the first three years of its construction, the newly proposed EVP-SANICLAY model provides predictions qualitatively and quantitatively consistent with the field measurements. The long-term settlement predictions are shown in Figures 7(e) and (f). The results in these figures illustrate that the consolidation finishes after about 100 and 300 days for the MC and MCC models, respectively, as the settlement increase for both models stops at those times. However, evidently for the EVP model it takes longer for the excess PWP to dissipate. This results in predictions more consistent with the field measurements in long-term. Figure 7(f), also illustrates that this consistency is well-preserved for 800 days and then the numerical predictions deviate from the field measurements as the rate of the settlement seems to change. This can be due to the fact that the model parameters are considered to remain constant with time, while in reality these parameters are interconnected and can vary as the settlement develops. It is also worth mentioning that such a deviation is less pronounced in a shorter time window, Figure 7(d), which suggests that the perception of divergence can partly be due to the way the results are visualized. Moreover, the final field measurements do not guarantee that the embankment settlement will necessarily follow the new trend. Assuming that the settlement will continue at the new rate after 800 days, capturing such abrupt changes will be out of the scope of the present model. Considering the fact that the viscosity parameters N and μ do not possess a unique value, adopting different values for these parameters, a prediction zone can be defined that encases the field

measurements, Figure 7(e). However, this alternative will be more sensible when Class A predictions are sought.

It is worth mentioning that compared to several other soft soil test embankments reported in the literature, the Ballina test embankment has shown considerably more settlements. For instance, over the same time period, compared to Murro [36], Saint Alban [37] and Tavan road [38] the settlement of this test embankment is about 3, 3, and 6 times greater, respectively. It might be attributed to the lower OCR value of the Ballina clay which results in larger plastic deformations. In order to highlight the contribution of different natural characteristics of Ballina clay on the embankment settlement prediction, the Class C simulations have been repeated using the SANICLAY model without consideration of soil structure, and using the structured SANICLAY model (with destructuration law). These simulations, along with those of MCC and EVP-SANICLAY models are shown in Figure 8. From this figure, it is clear that the consideration of Ballina clay's fabric anisotropy alone does not provide much improved predictions compared to the commonly used MCC model. However, the clay's structure and its viscosity appear to have considerable influence on its response, as when the effects of these characteristics are taken into account within the constitutive model the predictions are notably improved, particularly when the time effects (i.e., viscosity effects) are considered.

The Class A and Class C predicted vertical displacements with time, at different depths, are shown in Figures 9(a) and (b), respectively. These results are corresponding to the experimental measurements of the in-depth magnetic extensometers. These numerical predictions illustrate that the top soil layers of the embankment experience larger vertical displacements [36]. The new numerical results are qualitatively similar to their Class A counterpart and their quantitative differences can be attributed to their different model parameters.

Figures 10(a), (c) and (e) show the Class A predictions of total PWP variations at the nodes corresponding to the VWP6a (Vibrating Wire Piezometer), VWP6b and VWP6c of the

instrumented embankment, respectively. The corresponding Class C predictions and field measurement data are shown in Figures 10(b), (d) and (f), respectively. The field data shows that, as the depth increases (2m for VWP6a, 6m for VWP6b and 10m for VWP6c), the total PWP increases as well. Such an increase is captured in Class A and Class C simulations. For all the three depths, the numerical simulations, using MC, MCC and EVP-SANICLAY models, predicted that the total PWP initially increases during embankment construction (first 65 days) and then it gradually dissipates with time for the next 940 days. This trend can also be seen in field measurements by VWP6b and c. For VWP6a, such a trend exists just for the first 200 days and after that, the measured total PWP gradually increases. The comparison between the numerical results of these three models shows that in terms of PWP dissipation all predictions are qualitatively similar except that in general EVP predicts higher PWP values. However, despite qualitative agreement between numerical and experimental results, Figure 10 shows considerable quantitative differences between Class C predictions and their corresponding field data. Generally speaking, quantitatively accurate prediction of PWP variations is a challenging task which is usually accompanied with discrepancies between field measurements and numerical results. One of the most probable reasons of this can be the intrinsic limitations of the numerical model. The embankment is simulated adopting a 2D plane strain condition which requires a 2D equivalent of the 3D axisymmetric vertical drains which can result in different local pore pressure distributions. For example, in Figure 10(a), the dissipation of the PWP in the numerical results occurs at a greater rate of what is reflected by field measurements, which can be due to the fact that the equivalent permeability used in the models is greater than that of the real soil and PVD system. Identifying the actual reasons for differences between the field measured data and numerical results for PWP, would require more analyses and specific field data. It is also possible that the model used in this study to evaluate equivalent permeability may not represent the actual behavior of the subsoil [34].

Computers and Geotechnics. Submitted January 2017; Published January 2018.
http://dx.doi.org/10.1016/j.compgeo.2017.05.013

The Class A and C predictions of total horizontal pressure variations with time at different depths are shown in Figures 11(a) and (b), respectively. The experimental and their numerical counterparts are corresponding to the measurements of the 1st to 4th push in pressure cells (PIPC1-4). As it can be seen, for the PIPC1 which is installed in 0.35m depth, the total horizontal pressure increases during construction and then, after a small reduction, it remains constant. Similar trend can be seen in the numerical results as well. While the overall total horizontal pressure increases with depth, comparable patterns can be observed for other PIPCs data except that there is less fluctuation in the numerical results for lower depths. Both Class A and C predictions show analogous trend of variations and the differences are mainly due to different model parameter values adopted.

Figures 12(a) and (b) show Class A and C predictions of lateral deformation profiles at the toe of the embankment, respectively. Similarly the numerical predictions of surface settlement troughs are presented in Figures 12(c) and (d). The comparison of the numerical results of lateral deformations (which are corresponding to the measurements of the inclinometer INCLO2) shows that, while the MC model underestimates the embankment responses, the MCC and EVP-SANICLAY models overestimate short-term lateral deformations. Figure 12(b) also illustrates that the long-term predictions of EVP-SANICLAY model are in good agreement with the field measurements; whereas, the other two models fail to provide reasonable predictions, in particular the MC model underestimates the long-term lateral deformations. Compared to other test embankments over soft clayey soils that have been reported in the literature, the lateral deformations of the current embankment occur at a greater rate. For example, while the lateral deformation of the Ballina embankment doubles in extent within 3.5 years from its construction, such a deformation takes place within 8.5 years for the Murro embankment [39] and 4.5 years for the St. Alban embankment B [40]. The comparison between Figures 12(a) and (b) also shows that, whereas for Class A analyses MCC model

predictions of lateral deformations in short-term (i.e., for the first 10 weeks) surpassed those of the EVP model, for Class C analyses the EVP model always predicts lateral deformations higher than those from the MCC model. Figure 12(c) and (d) show that, immediately after the construction, surface settlements are small outside of the embankment area. Figure 12(d) also illustrates that the maximum surface settlement after 1090 days from the embankment construction is almost 4 times larger than that immediately after the construction. For both cases, the maximum vertical deformation is predicted to be directly underneath the centerline of the embankment. All of these predictions are consistent with the field data which were measured using hydrostatic profile gauge 1 (HPG1). Qualitatively, similar patterns can be observed for surface settlements and lateral deformations of other embankments (e.g. [41]). Comparable results can also be seen in Figure 12(c) except that the numerical predictions have less quantitative consistency with the field data.

5. CONCLUSIONS

The Class C predictions of time-dependent responses for a test embankment equipped with PVDs was provided using the EVP-SANICLAY model modified with a new and improved RH law. The model parameters were evaluated and calibrated using detailed experimental results of CRS and triaxial tests. The model parameter values and their changes compared to those used for Class A simulations were discussed. Apart from the model parameters, for the Class C predictions, the effect of PVDs was modeled through evaluation of an equivalent vertical permeability for the PVD-improved soil and also the variations of preconsolidation ratio with depth was taken into account using POP**.** Then, the calibrated model was implemented as a user defined soil model in the PLAXIS software to perform the numerical simulations of the test embankment. To better highlight the advantages of considering natural features of soil behavior, such as anisotropy, structure, and time effects, on the reliability of the numerical

predictions, the embankment was also simulated using two commonly used models in practice, namely MC and MCC models. The comparison of the numerical predictions using the EVP-SANICLAY model with those obtained using the classical models and the field measurements showed that while the MC and MCC models failed to capture the field observed short-term and long-term deformations, the EVP-SANICLAY model provided notably improved predictions of embankment responses which were reasonably comparable with the field measurements. The discrepancies with field measurements which appeared in some results highlighted the intrinsic limitations of routine numerical modeling approaches for simulation of complicated hydro-mechanical behavior of soft soil deposits overlain by a geo-structure such as embankment. Nevertheless, the present study showed that in order to gain better numerical accuracy in practical boundary value level simulations, the new elasto-viscoplastic model, that takes into consideration some of the fundamental features of natural soil behavior, can be used following a standard and straightforward calibration procedure.

Acknowledgments

The financial support of the RFCS project SLOPES (Contract RFCR-CT-2015-00001) funded by the European Commission is gratefully acknowledged. The second author also expresses appreciation to the financial support from The Vietnamese Ministry of Education and The University of Nottingham. The last author acknowledges financial support from the Natural Sciences and Engineering Research Council of Canada (NSERC).

REFERENCES

[1] Sekiguchi H, Ohta H. Induced anisotoropy and time dependency in clay. In: Proc 9th Int Conf Soil Mech Found Eng, Tokyo, 11–15 July 1977. p. 229–38.

[2] Dafalias YF. An anisotropic critical state soil plasticity model. Mech Res Commun 1986;13(6):341–7.

[3] Dafalias YF. An anisotropic critical state clay plasticity model. In: Proc 2nd Int Conf Constitutive Laws for Engineering Materials – Theory and Applications. Tucson, 5–8 January 1987. p. 513–21.

[4] Dafalias YF, Manzari MT, Papadimitriou AG. SANICLAY: simple anisotropic clay plasticity model. Int J Numer Anal Meth Geomech 2006;30(12):1231–57.

[5] Taiebat M, Dafalias YF, Peek R. A destructuration theory and its application to SANICLAY model. Int J Numer Anal Meth Geomech 2010;34(10):1009–40.

[6] Taiebat M. Advanced elastic-plastic constitutive and numerical modeling in geomechanics. PhD Thesis, University of California, Davis; 2008.

[7] Seidalinov G, Taiebat M. Bounding surface SANICLAY plasticity model for cyclic clay behavior. Int J Numer Anal Meth Geomech 2014;38(7):702–24.

[8] Taiebat M, Kaynia AM, Dafalias, YF. Application of an anisotropic constitutive model for structured clay to seismic slope stability. J Geotech Geoenviron Eng 2011;137(5):492–504.

[9] Seidalinov G, Taiebat M. Propagation of seismic waves through saturated soft clay deposits: Constitutive and numerical modeling. In: Proc 14th Conf Int Asso Comput Meth Adv Geomech, Kyoto, 22–25 September 2014. p. 285–90.

[10] Tavenas F, Leroueil S, Rochelle PL, Roy M. Creep behaviour of an undisturbed lightly overconsolidated clay. Can Geotech J 1978;15(3):402–23.

[11] Leroueil S, Kabbaj M, Tavenas F, Bouchard R. Stress–strain–strain rate relation for the compressibility of sensitive natural clays. Géotechnique 1985;35(2):159–80.

[12] Lefebvre G, LeBoeuf D. Rate effects and cyclic loading of sensitive clays. J Geotech Eng 1987;113(5):476–89.

Computers and Geotechnics. Submitted January 2017; Published January 2018.
http://dx.doi.org/10.1016/j.compgeo.2017.05.013

[13] Augustesen A, Liingaard M, Lade PV. Evaluation of time-dependent behavior of soils. Int J Geomech 2004;4(3):137–56..

[14] Naghdi PM, Murch SA. On the mechanical behavior of viscoelastic/plastic solids. J Appl Mech 1963;30(3):321–8.

[15] Perzyna P. Fundamental problems in viscoplasticity. Adv Appl Mech 1966;9:244–377.

[16] Rezania M, Taiebat M, Poletti E. A viscoplastic SANICLAY model for natural soft soils. Comput Geotech 2016;73:128–41.

[17] Fodil A, Aloulou W, Hicher PY. Viscoplastic behaviour of soft clay. Géotechnique 1997;47(3):581–91.

[18] Dafalias YF, Taiebat M. Anatomy of rotational hardening in clay plasticity. Géotechnique 2013;63(16):1406–18.

[19] Pineda JA, Suwal LP, Kelly RB, Bates L, Sloan SW. Characterisation of Ballina clay. Géotechnique 2016;66(7):556–77.

[20] Rezania M, Nguyen H, Zanganeh H, Taiebat M. Modelling the rate-dependent behaviour of an embankment on soft Ballina clay using an anisotropic elastic-viscoplastic soil model. In: Embankment Prediction Symposium, Newcastle, 12–13 September 2016. p. 314–27.

[21] Embankment Prediction Symposium, http://cgse.edu.au/eps2016. 2016.

[22] Wheeler SJ, Näätänen A, Karstunen M, Lojander M. An anisotropic elastoplastic model for soft clays. Can Geotech J 2003;40(2):403–18.

[23] Plaxis (2014) PLAXIS 2D Anniversary Edition - Reference Manual. Plaxis bv, Delft; 2014.

[24] Sivasithamparam N, Rezania M. The comparison of modelling inherent and evolving anisotropy on the behaviour of a full-scale embankment. Int J Geotech Eng 2016. http://dx.doi.org/10.1080/19386362.2016.1221575.

[25] Yildiz A, Karstunen M, Krenn H. Effect of anisotropy and destructuration on behavior of Haarajoki test embankment. Int J Geomech 2009;9(4):153–68.

[26] Hird CC, Pyrah IC, Russel D. Finite element modelling of vertical drains beneath embankments on soft ground. Géotechnique 1992;42(3):499–511.

[27] Rixner JJ, Kramer SR, Smith AD. Prefabricated vertical drains, Vol. II: Summary of research effort. Federal Highway Administration Research Report No. FHWA/RD-86/169. Washington; 1986.

[28] Abuel-Naga H, Bouazza A. Equivalent diameter of a prefabricated vertical drain. Geotext Geomembr 2009;27(3):227–31.

[29] Bo M, Bawajee R, Chu J, Choa V. Investigation of smear zone around vertical drain. In: Proc 3rd Int Conf Ground Improvement Techniques, Singapore, 25–26 September 2000. p. 109–14.

[30] Xiao D. Consolidation of soft clay using vertical drains. PhD Thesis, Nanyang Technological University, Singapore; 2011.

[31] Madhav MR, Park Y-M, Miura N. Modelling and study of smear zones around band shaped drains. Soils Found 1993;33(4):135–47.

[32] Bergado DT, Mukherjee K, Alfaro MC, Balasubramaniam AS. Prediction of vertical-band-drain performance by the finite-element method. Geotext Geomembr 1993;12(6):567–86.

[33] Olson RE. Settlement of embankments on soft clays: (The Thirty-First Terzaghi Lecture). J Geotech Geoenviron Eng 1998;124(8):659–69.

[34] Chai J-C, Shen S-L, Miura N, Bergado DT. Simple method of modeling PVD-improved subsoil. J Geotech Geoenviron Eng 2001;127(11):965–72.

[35] Taylor DW. Fundamentals of soil mechanics. Wiley; 1948.

[36] Karstunen M, Krenn H, Wheeler SJ, Koskinen M, Zentar R. Effect of anisotropy and destructuration on the behavior of Murro test embankment. Int J Geomech 2005;5(2):87–97.

[37] Rochelle PL, Trak B, Tavenas F, Roy M. Failure of a test embankment on a sensitive Champlain clay deposit. Can Geotech J 1974;11(1):142–64.

[38] Manzari MT, Yonten K. On implementation and performance of an anisotropic constitutive model for clays. Int J Comput Meth 2014;11(2):1342009.

[39] karstunen M, Yin Z-Y. Modelling time-dependent behaviour of Murro test embankment. Géotechnique 2010;60(10):735–49.

[40] Tavenas F, Mieussens C, Bourges F. Lateral displacements in clay foundations under embankments. Can Geotech J 1979;16(3):532–50.

[41] Karstunen M, Rezania M, Sivasithamparam N, Yin Z-Y. Comparison of anisotropic rate-dependent models for modeling consolidation of soft clays. Int J Geomech 2015;15(5):A4014003.

Computers and Geotechnics. Submitted January 2017; Published January 2018.
http://dx.doi.org/10.1016/j.compgeo.2017.05.013

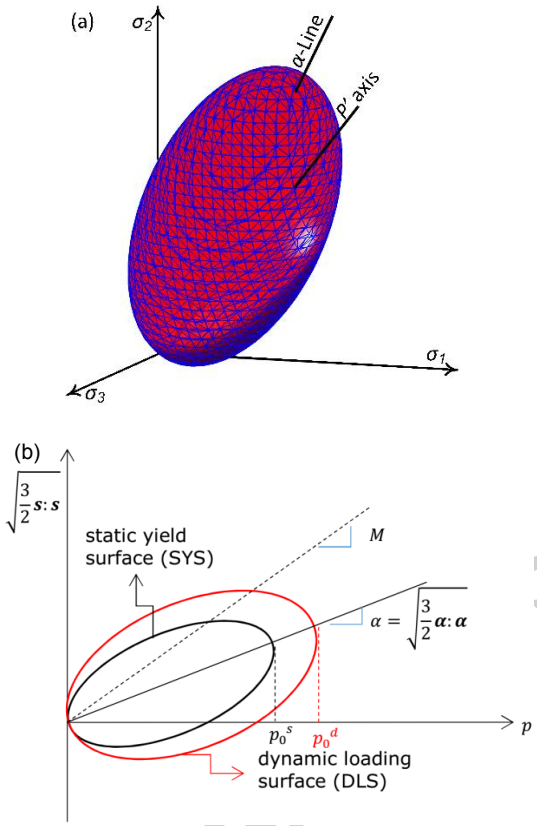

Figure 1: Schematic depiction of the EVP-SANICLAY model in (a) the general stress space; (b) triaxial stress space.

Computers and Geotechnics. Submitted January 2017; Published January 2018.
http://dx.doi.org/10.1016/j.compgeo.2017.05.013

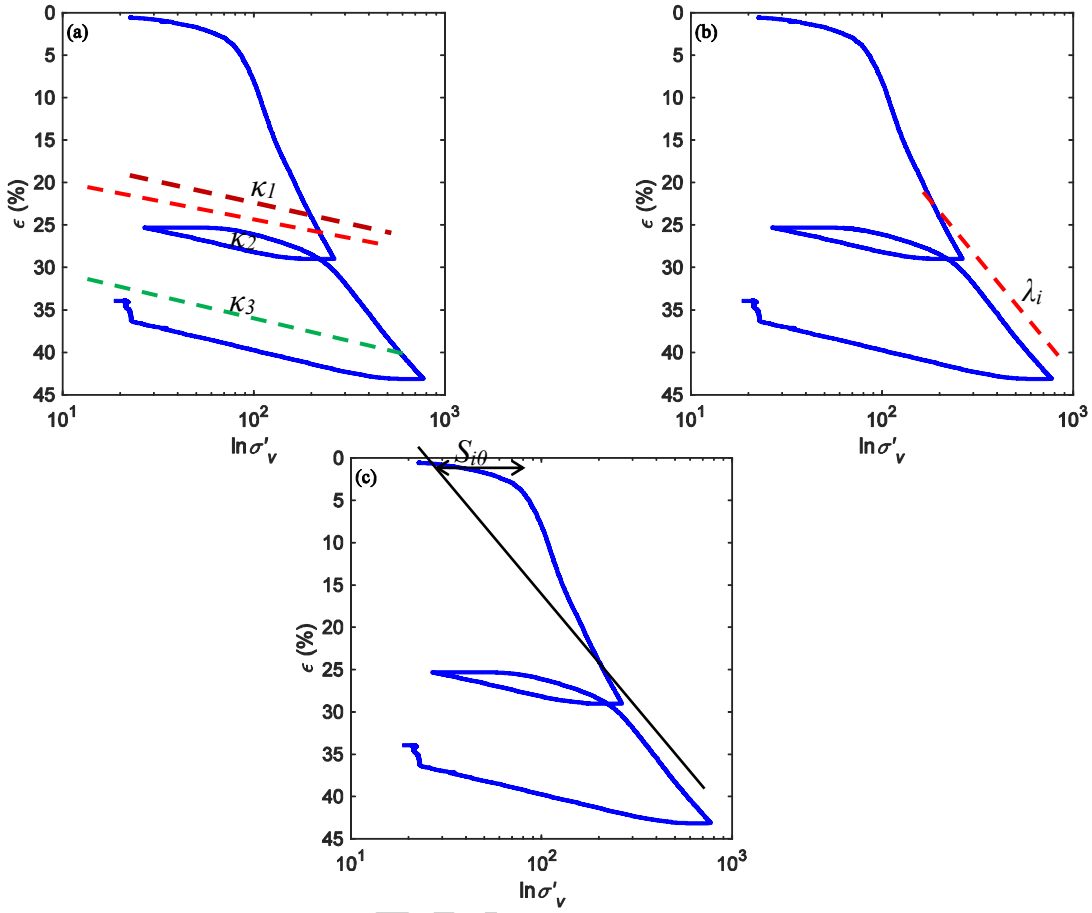

Figure 2: Evaluation of (a) κ (b) λ_i and (c) S_{io} using CRS test for a sample taken from depth of 6.63m.

Computers and Geotechnics. Submitted January 2017; Published January 2018.
http://dx.doi.org/10.1016/j.compgeo.2017.05.013

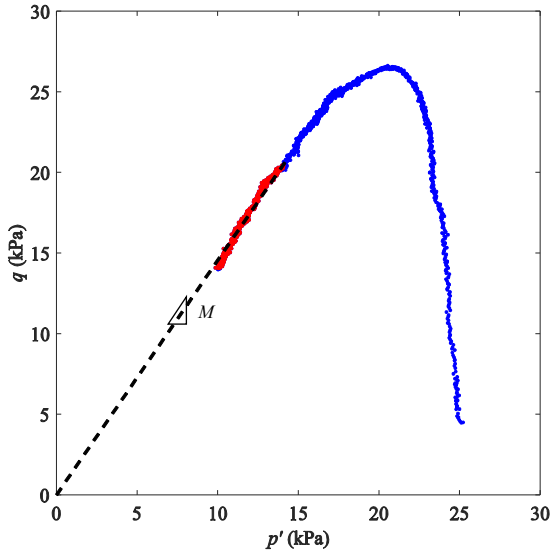

Figure 3: Evaluation of M using triaxial test data for a sample taken from depth of 6.63m.

Computers and Geotechnics. Submitted January 2017; Published January 2018.
http://dx.doi.org/10.1016/j.compgeo.2017.05.013

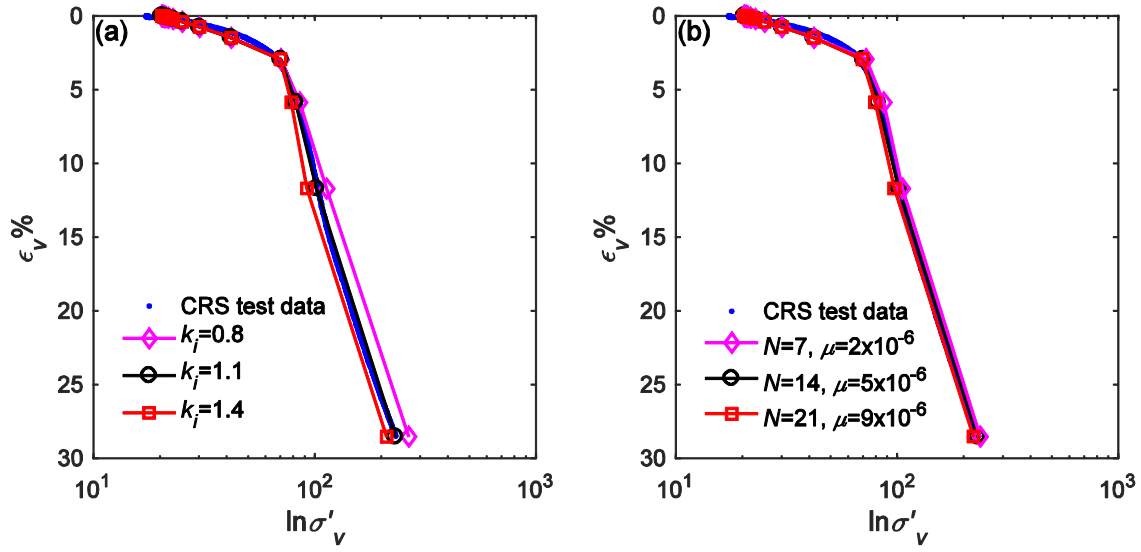

Figure 4: Calibration of (a) k_i (b) N and μ using CRS test for a sample taken from depth of 6.63m.

Computers and Geotechnics. Submitted January 2017; Published January 2018.
http://dx.doi.org/10.1016/j.compgeo.2017.05.013

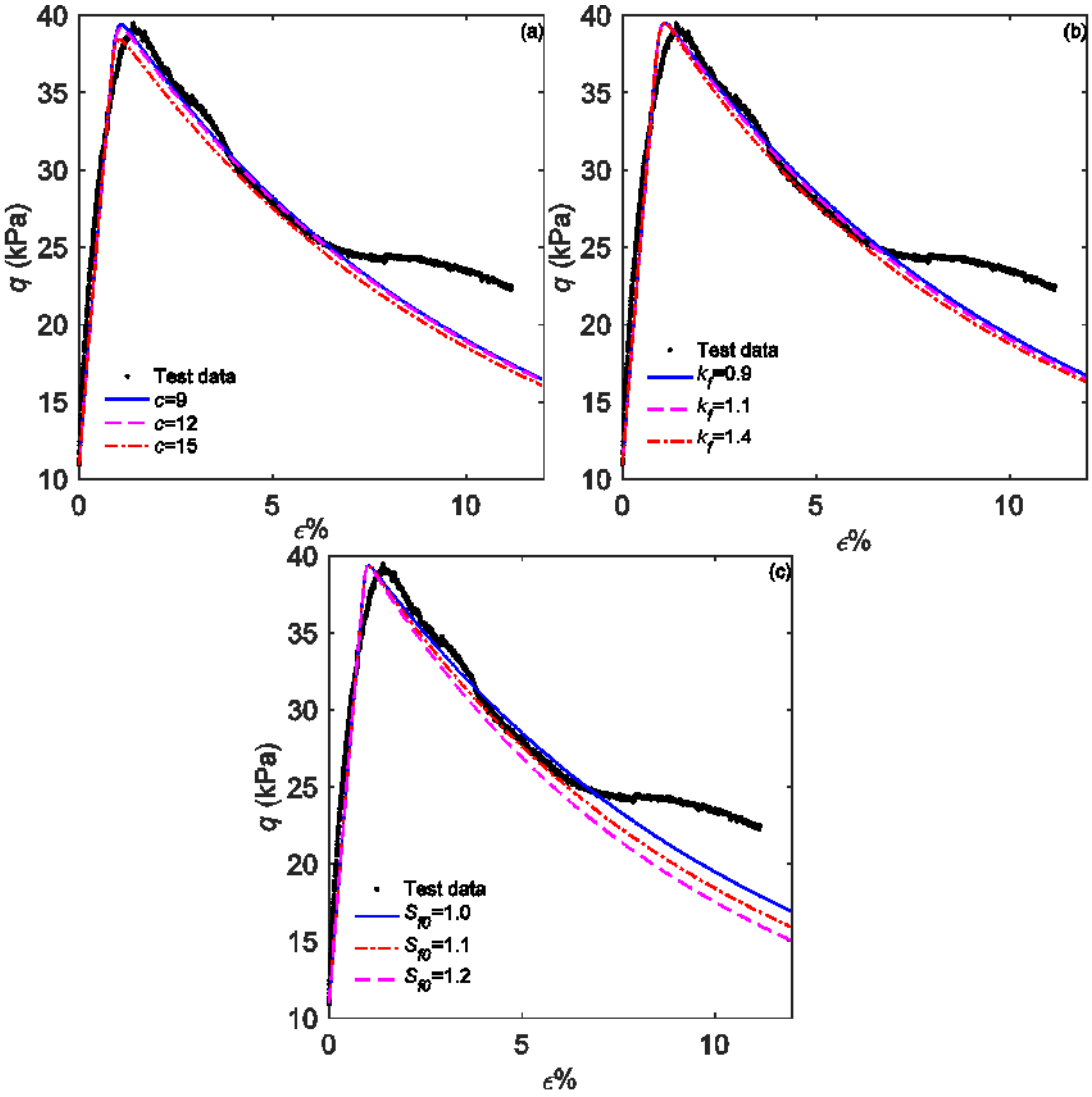

Figure 5: Calibration of (a) c (b) k_f and (c) S_{f0} using triaxial test data for a sample taken from 6.63m depth.

Computers and Geotechnics. Submitted January 2017; Published January 2018.
http://dx.doi.org/10.1016/j.compgeo.2017.05.013

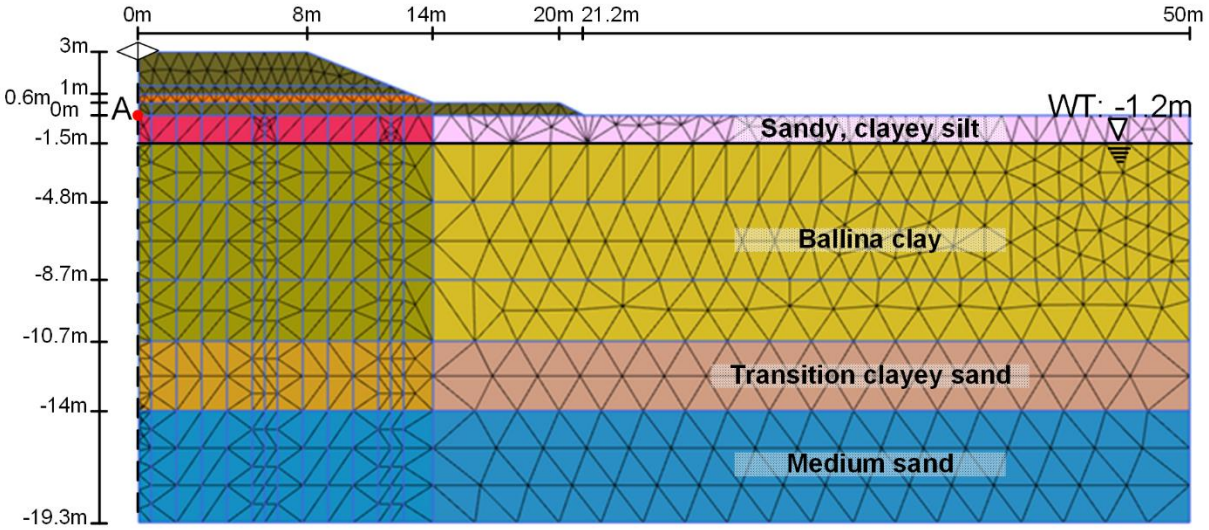

Figure 6: Geometry of the model embankment and the finite element mesh adopted.

Computers and Geotechnics. Submitted January 2017; Published January 2018.
http://dx.doi.org/10.1016/j.compgeo.2017.05.013

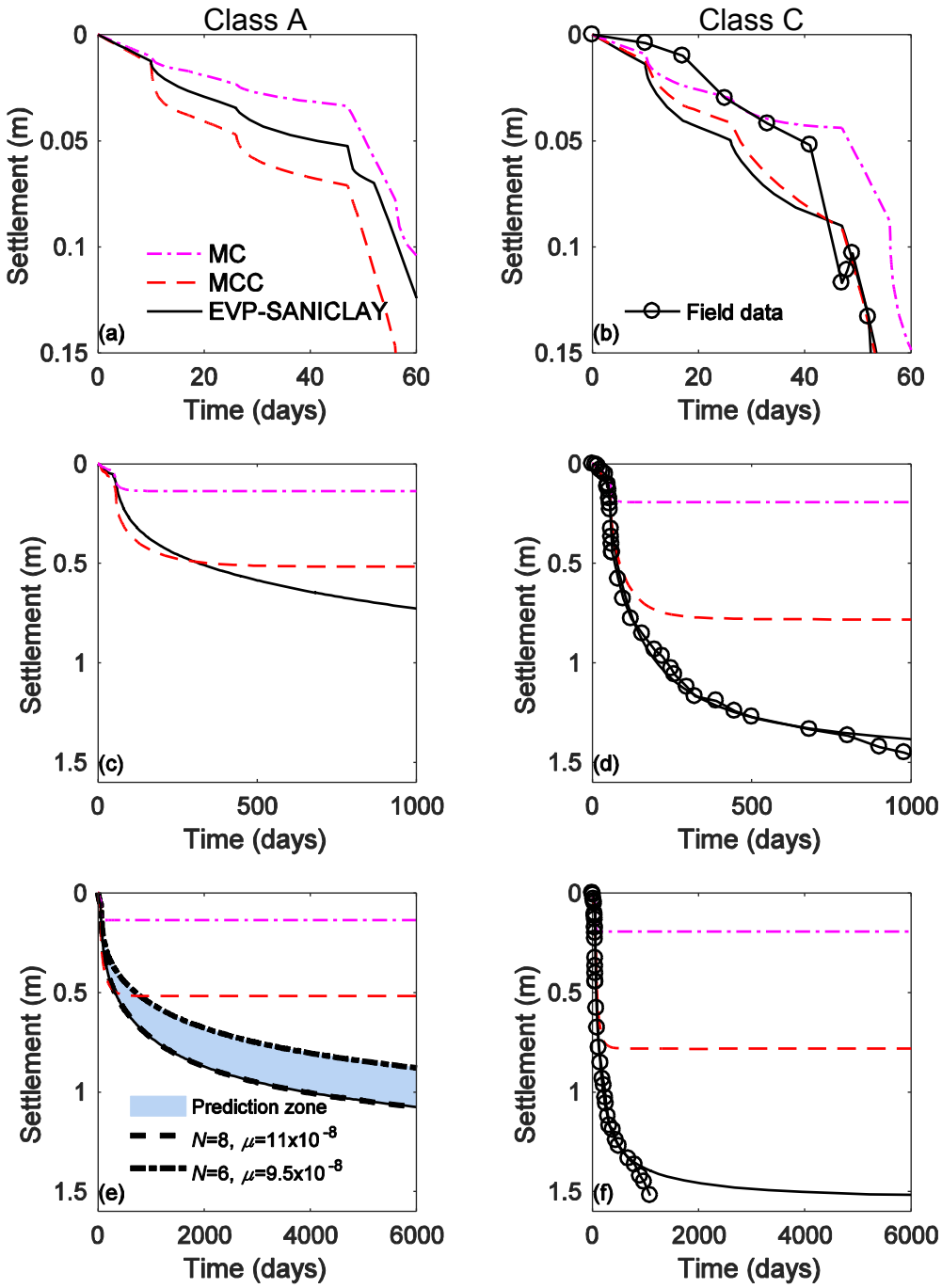

Figure 7: Numerical predictions of time-settlement (a) and (b) during construction, (c) and (d) after two years, (e) and (f) in long term.

Computers and Geotechnics. Submitted January 2017; Published January 2018.
http://dx.doi.org/10.1016/j.compgeo.2017.05.013

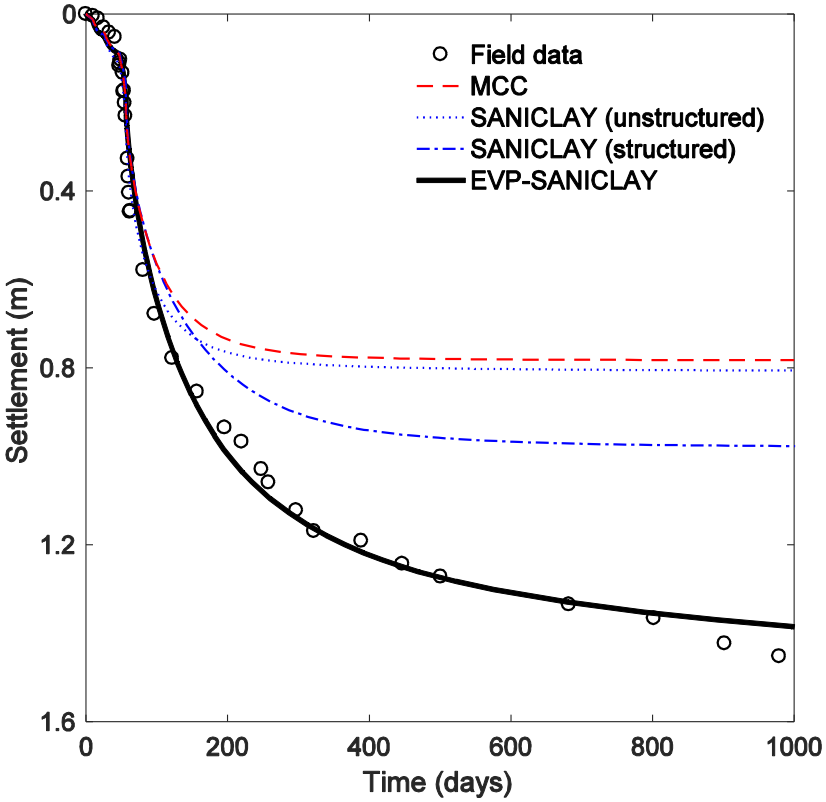

Figure 8: The effect of soil characteristics on the numerical predictions of time-settlement.

Computers and Geotechnics. Submitted January 2017; Published January 2018.
http://dx.doi.org/10.1016/j.compgeo.2017.05.013

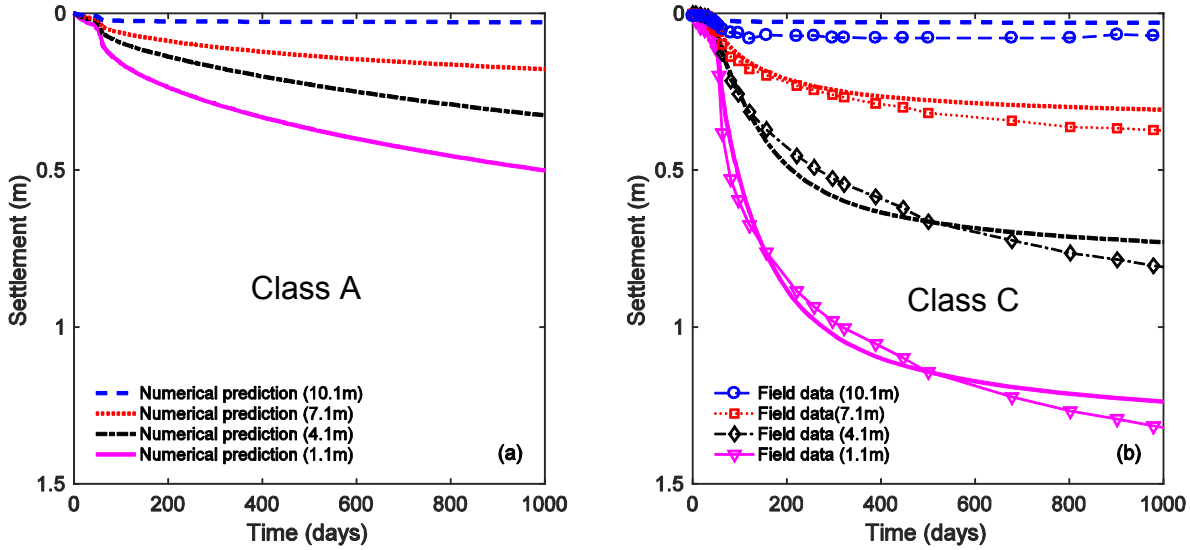

Figure 9: Numerical predictions of time-settlement at different depths.

Computers and Geotechnics. Submitted January 2017; Published January 2018.
http://dx.doi.org/10.1016/j.compgeo.2017.05.013

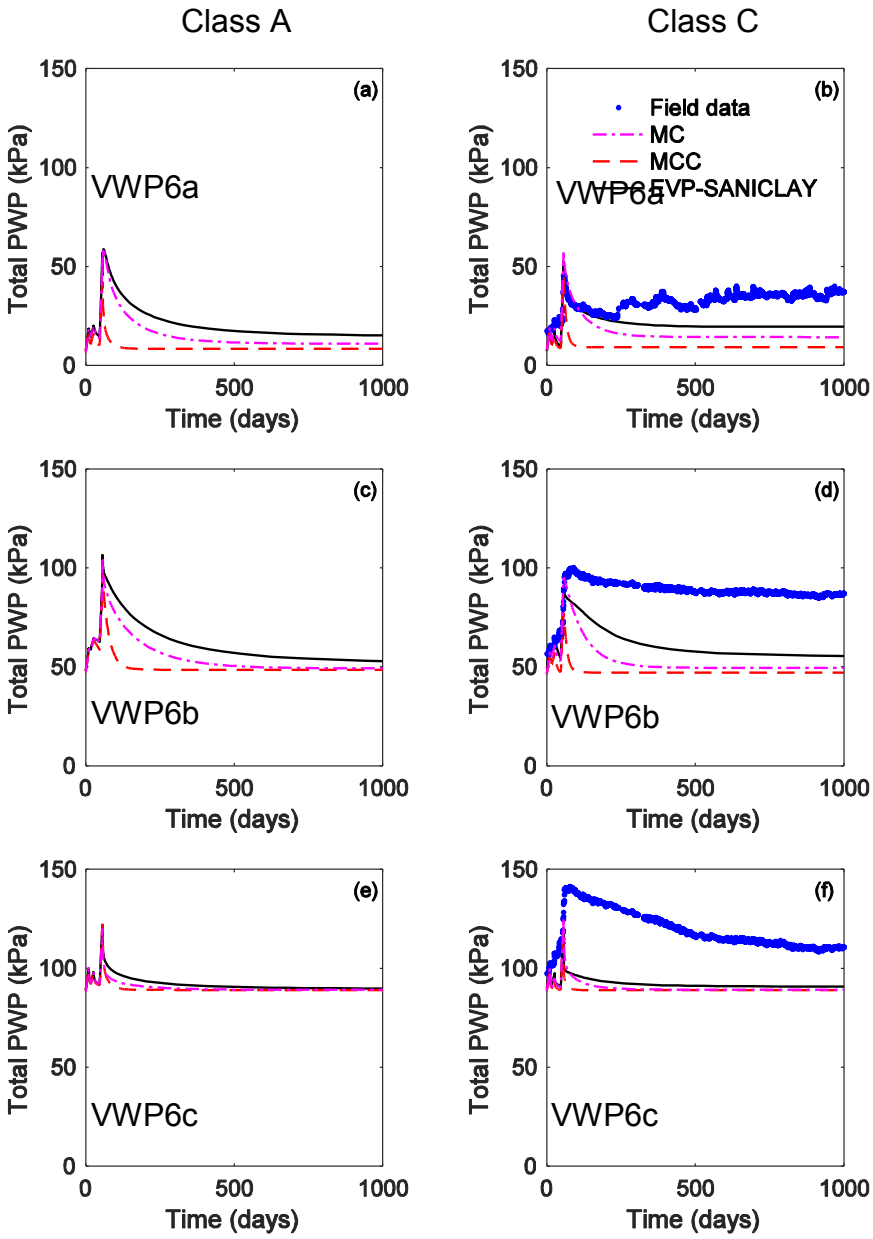

Figure 10: Numerical predictions of Excess PWP variations.

Computers and Geotechnics. Submitted January 2017; Published January 2018.
http://dx.doi.org/10.1016/j.compgeo.2017.05.013

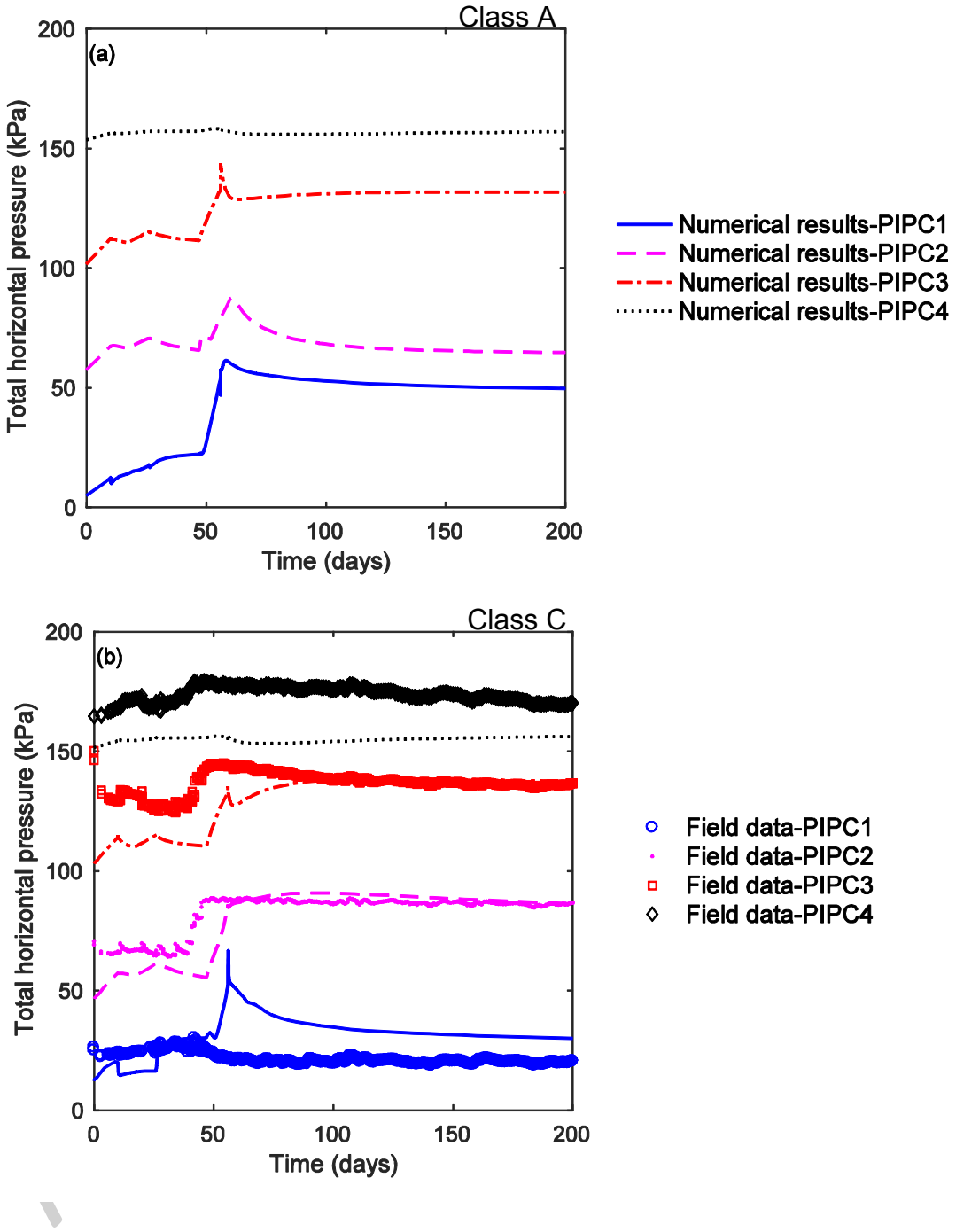

Figure 11: Numerical predictions of total horizontal pressure.

Computers and Geotechnics. Submitted January 2017; Published January 2018.
http://dx.doi.org/10.1016/j.compgeo.2017.05.013

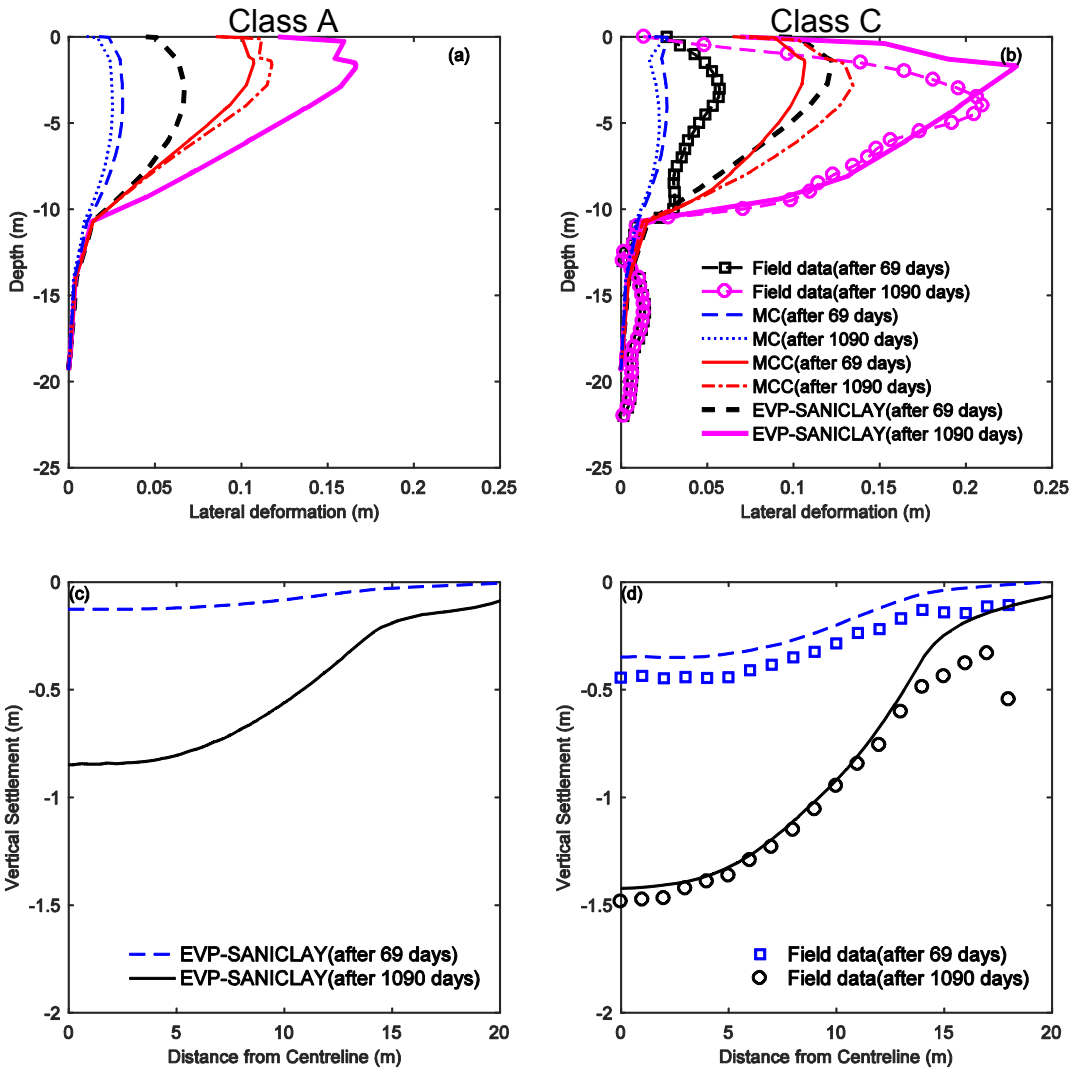

Figure 12: Numerical predictions of (a) and (b), lateral displacement under the toe and, (c) and (d) surface settlement of the embankment.

Computers and Geotechnics. Submitted January 2017; Published January 2018.
http://dx.doi.org/10.1016/j.compgeo.2017.05.013

Table 1: Constants of the modified EVP-SANICLAY model adopted for Ballina test embankment.

Model constant		Top sandy-clayey silt		Ballina Clay	
		Class A	Class C	Class A	Class C
Elasticity	κ	0.007	0.007	0.069	0.099
	v	0.25	0.25	0.27	0.27
Critical state	M	1.033	1.033	1.47	1.27
	λ_i	0.13	0.13	0.37	0.4
Rotational hardening	c	13	13	12	12
	$z = s$	2	2	2	2
Destructuration	k_i	1	1	1.13	1.1
	k_f	1	1	1.17	1.2
Viscosity	N	2	2	7	14
	μ (s^{-1})	2×10^{-8}	2×10^{-8}	1.03×10^{-7}	5×10^{-6}
Initial state	e_0	1.09	1.09	2.52	2.85
	OCR/POP(kPa)	3.09(OCR)	21.9(POP)	1.86(OCR)	11.7(POP)
	α_0	0.02	0.02	0.21	0.236
	S_{i0}	1	1	3.1	3.3
	S_{f0}	1	1	1.1	1.1

Computers and Geotechnics. Submitted January 2017; Published January 2018.
http://dx.doi.org/10.1016/j.compgeo.2017.05.013

Table 2: MC Model parameter values adopted for Ballina test embankment.

Model constant		Fill (MC)	Sand (MC)	Top sandy-clayey silt		Ballina Clay		Transition Sand (MC)	Sand (MC)
				Class A (MC)	Class C (MCC)	Class A (MC)	Class C (MC)		
Elasticity	E' (kPa)	25000	20000	5000	κ=0.007	4226	4226	10000	40000
	v	0.25	0.25	0.25	0.25	0.27	0.27	0.25	0.25
Strength	c' (kPa)	1	0	15	M=1.033	14	14	2	1
	φ' (deg)	38	33	34	λ=0.13	36	36	30	35
Initial state	e_0	1	0.5	1.09	1.09	2.52	2.85	0.5	0.5
					POP=21.6 (kpa)				

Computers and Geotechnics. Submitted January 2017; Published January 2018.
http://dx.doi.org/10.1016/j.compgeo.2017.05.013

Table 3: Coefficient of permeability values adopted for Ballina test embankment.

Permeability		Fill	Sand	Top sandy-clayey silt		Ballina Clay		Transition sand		Sand
				Class A	Class C	Class A	Class C	Class A	Class C	
k_{hv}	m/day	0.0475	193	6.4×10^{-3}	6.4×10^{-3}	4.84×10^{-4}	4.84×10^{-4}	4.75×10^{-2}	4.75×10^{-2}	1.93×10^{2}
k_{eh}	m/day	N/A	N/A	1.02×10^{-4}	1.16×10^{-4}	7.96×10^{-6}	8.78×10^{-6}	7.54×10^{-4}	8.61×10^{-4}	N/A
k_{ev}	m/day	N/A	N/A	Drain modelled	1.63×10^{-2}	Drain modelled	3.78×10^{-3}	Drain modelled	5.84×10^{-2}	N/A
c_k		N/A	N/A	0.166	0.166	0.766	0.766	N/A	N/A	N/A

Computers and Geotechnics. Submitted January 2017; Published January 2018.
http://dx.doi.org/10.1016/j.compgeo.2017.05.013

Table 4: MCC Model parameter values adopted for Ballina test embankment.

Model constant		Fill (MC)	Sand (MC)	Top sandy-clayey silt		Ballina Clay		Transition Sand (MC)	Sand (MC)
				Class A (MCC)	Class C (MCC)	Class A (MCC)	Class C (MCC)		
Elasticity	E' (kPa)	25000	20000	κ=0.007	κ=0.007	κ=0.069	κ=0.099	10000	40000
	v	0.25	0.25	0.25	0.25	0.27	0.27	0.25	0.25
Strength	c' (kPa)	1	0	M=1.033	M=1.033	M=1.47	M=1.27	2	1
	φ'(deg)	38	33	λ=0.13	λ =0.13	λ=0.37	λ =0.4	30	35
Initial state	e_0	1	0.5	1.09	1.09	2.52	2.85	0.5	0.5
	OCR/POP(kPa)			OCR=3.09	POP=21.6	OCR=1.86	POP=11.7		